Chem Catalysis

CellPress

Article

A general Ca-MOM platform with enhanced acid-base stability for enzyme biocatalysis

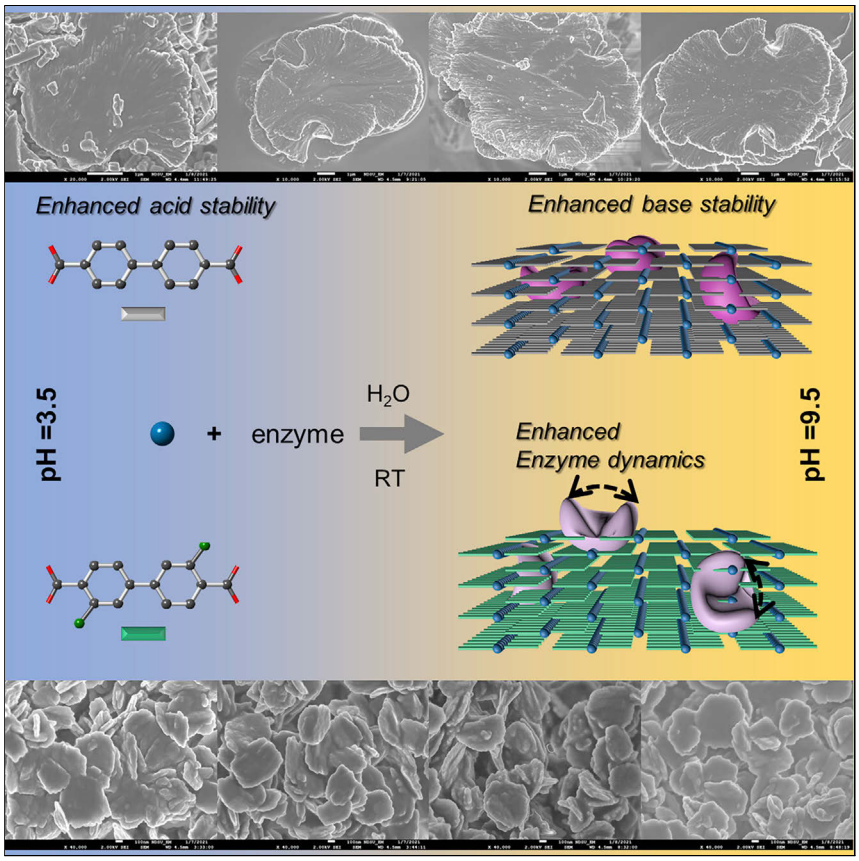

By co-precipitation of enzymes, Ca^{2+}, and carboxylate ligands, we discovered the formation of biocomposites that are stable under a wide range of pHs (3.5–9.5). The catalytic activity was demonstrated on four enzymes with different sizes and isoelectric points. SDSL-EPR then revealed enhanced backbone dynamics of enzymes upon encapsulation in one of our biocomposites. The developed platform can be generalized to immobilize arbitrary enzymes and carry out catalytic reactions under the desired pH of the host enzyme.

Yanxiong Pan, Qiaobin Li, Hui Li, ..., Zhiping Lai, Bingcan Chen, Zhongyu Yang

zhiping.lai@kaust.edu.sa (Z.L.)
bingcan.chen@ndsu.edu (B.C.)
zhongyu.yang@ndsu.edu (Z.Y.)

Highlights

Ca^{2+} and carboxylate ligands immobilize enzymes via co-precipitation in water

Enzyme@Ca-MOF biocomposites are stable under pH 3.7–9.5 and catalytically active

Biocatalysis is possible under a needed pH for optimal performance on our composites

SDSL and EPR are combined to elucidate enzymes' behavior in our composites

Pan et al., Chem Catalysis 1, 146–161
June 17, 2021
https://doi.org/10.1016/j.checat.2021.03.001

CellPress

Chem Catalysis

Article

A general Ca-MOM platform with enhanced acid-base stability for enzyme biocatalysis

Yanxiong Pan,[1] Qiaobin Li,[1] Hui Li,[2] Jasmin Farmakes,[1] Angel Ugrinov,[1] Xiao Zhu,[3] Zhiping Lai,[4,*] Bingcan Chen,[2,*] and Zhongyu Yang[1,5,*]

SUMMARY

Co-precipitation of enzymes in metal-organic frameworks is a unique enzyme-immobilization strategy but is challenged by weak acid-base stability. To overcome this drawback, we discovered that Ca^{2+} can co-precipitate with carboxylate ligands and enzymes under ambient aqueous conditions and form enzyme@metal-organic material composites stable under a wide range of pHs (3.7–9.5). We proved this strategy on four enzymes with varied isoelectric points, molecular weights, and substrate sizes—lysozyme, lipase, glucose oxidase (GOx), and horseradish peroxidase (HRP)—as well as the cluster of HRP and GOx. Interestingly, the catalytic efficiency of the studied enzymes was found to depend on the ligand, probing the origins of which resulted in a correlation among enzyme backbone dynamics, ligand selection, and catalytic efficiency. Our approach resolved the long-lasting stability issue of aqueous-phase co-precipitation and can be generalized to biocatalysis with other enzymes to benefit both research and industry.

INTRODUCTION

Enzyme immobilization can improve enzyme reusability, align enzyme orientation, and even enhance the catalytic efficiency.[1–3] However, designing proper enzyme-hosting platforms remains a long-standing challenge. Nanoparticles offer high surface-to-volume ratios (as compared with planar surfaces), but the immobilizing enzymes face leaching (if physically adsorbed) or chemical perturbation (if covalently linked).[4,5] Furthermore, surface immobilization offers insufficient enzyme protection and thus limits the enzyme reusability. Mesoporous materials offer enhanced enzyme protection but often suffer from poor substrate diffusivity. A unique porous material, the metal-organic framework (MOF), offers enhanced enzyme protection against reaction media with no enzyme leaching or chemical modification, improved substrate diffusivity and selectivity, and enhanced catalytic efficiency in certain cases.[6–13]

Thus far, the majority of enzyme@MOF applications have focused on enzymes smaller than or close to MOF apertures (a few nanometers); the substrate size also has to be small. Co-precipitation of enzymes with metal/ligand pairs (e.g., Zn^{2+}/imidazolate, the most common pair, and the recently developed metal/squarate pairs) overcomes the enzyme size limitation;[14–18] we recently also found this approach to be capable of exposing a portion of enzymes above the MOF surface, allowing for the catalysis of substrates that are significantly larger than MOF apertures.[19–21] However, the stability of the resultant composites formed via co-precipitation, especially

The bigger picture

Enzymes are optimal biocatalysts for research and industry because of their excellent selectivity and biocompatibility, yet their high costs limit the practical and broad applications. Co-precipitation of enzymes with certain metals and ligands can immobilize an enzyme with arbitrary molecular weight and/or substrate size and improve reusability, yet the resultant biocomposites often suffer from poor stability under acidic or basic conditions, limiting biocatalytic reactions under the desired pHs. This work discovers a series of metal-organic materials that can be generalized to immobilize arbitrary enzymes to form biocomposites that are stable under a wide pH range that covers the optimal pHs of most commonly seen enzymes. The ease of preparation and the ambient reaction conditions are additional advantages. The platform can potentially change how industry utilizes enzymes for various purposes with desired catalytic efficiency and sustainability.

under weakly acidic conditions, is not ideal, limiting the reaction medium to being basic. A promising success is a recent work using a polymer-zeolitic imidazolate framework (ZIF) hybrid to enhance ZIF stability under acidic conditions.[22] However, this approach does require some specific expertise and may not be suitable for general enzymes, especially metallo-enzymes, because imidazolate may chelate the endogenous metals. Mechanochemical encapsulation of powder-state enzymes in UiO-MOFs resulted in acid-stable enzyme@MOF composites,[23] yet these composites are unstable under basic conditions.[24] Given the high variety in enzymes and the wide range of their optimal pHs,[25] there is a critical need for a MOF that is simultaneously stable under both weakly acidic and basic pHs and can be generalized to enzymes with arbitrary surface charge, molecular weight, and/or substrate size.

In this work, we report an effective approach to simultaneously overcome all aforementioned barriers. Inspired by the recent Ca-MOF/metal-organic materials (MOMs),[26–32] we found that Ca^{2+} can form composites with enzymes and three carboxylate ligands—terephthalate sodium (BDC-Na_2), biphenyl-4,4′-dicarboxylate sodium (BPDC-Na_2), and 2,2′-diaminobiphenyl-4,4′-dicarboxylate sodium (NH_2-BPDC-Na_2)—under ambient conditions in water. Remarkably, the formed enzyme@Ca-MOMs were stable under both weakly acidic and basic pHs (3.7–9.5), as judged by the turbidity, crystallinity, and morphology. This finding overcomes the long-lasting stability problem of composites formed in the aqueous phase. We tested this platform on four enzymes with varied molecular weights, substrate sizes, and isoelectric points (IEPs): lysozyme (lys, 18.7 kDa; substrate, bacterial cell walls; IEP, 9.2; ~2.5 × 3.0 × 4.5 nm), lipase (53 kDa; substrate, esters; IEP, 5.8; ~3.0 × 3.2 × 6.6 nm), glucose oxidase (GOx, 80 kDa; substrate, glucose; IEP, 4.2; ~6.0 × 5.2 × 7.7 nm), and horseradish peroxidase (HRP, 44 kDa; substrate, H_2O_2; IEP, 3–9; ~3.7 × 4.3 × 6.4 nm). All four enzymes individually as well as the HRP/GOx cluster showed the expected catalytic activity against the corresponding substrates. Interestingly, we found that with the same amount of enzyme entrapped, the enzyme@Ca-NH_2-BPDC composite displayed a higher catalytic efficiency than Ca-BPDC and Ca-BDC for three of the four enzymes. To probe the cause of such activity difference, we took lys as a model and employed site-directed spin labeling (SDSL)-electron paramagnetic resonance (EPR) spectroscopy to probe the backbone dynamics of lys in each MOM.[33–39] SDSL-EPR is especially suitable for this investigation because it probes enzyme backbone dynamics at the residue level[33,40] regardless of the background matrices.[19–21] We found that in Ca-NH_2-BPDC, lys displayed higher backbone dynamics than Ca-BPDC and Ca-BDC on multiple protein sites. Thus, we speculate that enzyme intrinsic backbone flexibility is the highest in Ca-NH_2-BPDC for all enzymes, which explains the catalytic efficiency difference among different Ca-MOMs.

To the best of our knowledge, this is the first report on aqueous-phase, one-pot synthesis of enzyme@Ca-MOMs that are simultaneously stable under weakly acidic and basic conditions while preserving enzyme activities. Our approach can be generalized to other enzymes with arbitrary molecular weights and substrate sizes for biocatalysis under the needed pHs. The ease of operation and the ambient reaction conditions are also advantageous for industrial biocatalyst preparation.

RESULTS

Selection of metal and ligands

Aqueous-phase, one-pot co-precipitation can encapsulate enzymes with arbitrary sizes in MOFs to form enzyme@MOF composites (enzymes embedded in the

[1]Department of Chemistry and Biochemistry, North Dakota State University, Fargo, ND 58102, USA

[2]Department of Plant Sciences, North Dakota State University, Fargo, ND 58102, USA

[3]Research Computing, Information Technology at Purdue (ITaP), Purdue University, West Lafayette, IN 47907, USA

[4]King Abdullah University of Science and Technology, Thuwal, Saudi Arabia

[5]Lead contact

*Correspondence:
zhiping.lai@kaust.edu.sa (Z.L.),
bingcan.chen@ndsu.edu (B.C.),
zhongyu.yang@ndsu.edu (Z.Y.)

https://doi.org/10.1016/j.checat.2021.03.001

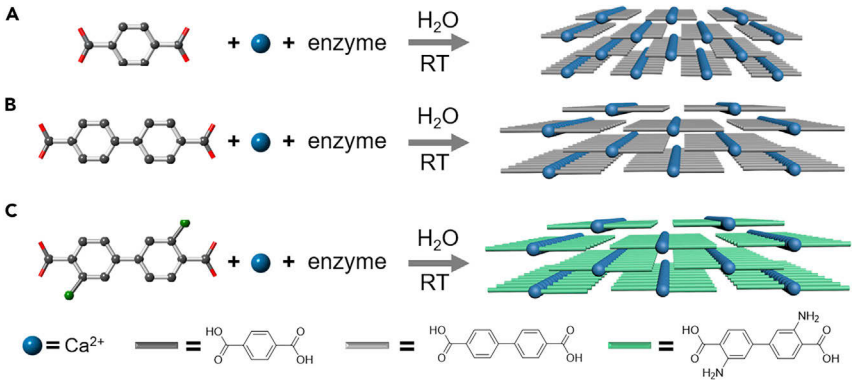

Figure 1. Synthetic schemes of the three Ca-MOMs discovered in this work

The stacking interactions of benzyl rings among different layers stabilize the overall structure for enzyme@Ca-BDC (A), Ca-BPDC (B), and Ca-NH_2-BPDC (C). Enzymes (purple) are encapsulated in crystal cavities.

materials) and allow for catalysis of large-size substrates.[19,41] However, composites formed in the aqueous phase are often challenged by poor stability, especially under (weakly) acidic or basic pHs. After scanning a number of metal/ligand pairs, we found that three carboxylate ligands—BDC-Na_2, BPDC-Na_2, and NH_2-BPDC-Na_2—can co-precipitate with Ca^{2+} and enzymes in water and form relatively stable composites over a wide range of pHs.

Synthesis and characterization of Ca-MOMs

We converted the –COOH groups of BDC, BPDC, and NH_2-BPDC to –COONa (Scheme S1) in order to improve their solubilities in water. Then, as shown in Figure 1, each ligand was mixed with Ca^{2+} and each enzyme under gentle mixing at room temperature in water. The unreacted species were removed via centrifugation-resuspension with water three times (see the supplemental information). The prepared composites were stored in water at 4°C for further use.

Under near-neutral pH, the enzyme@Ca-MOMs show varied morphology depending on the ligand as reported by scanning electron microscopy (SEM; for representative data of lys@Ca-MOMs, see row 3 in Figure 2A and Figure S1 for a larger scale). Lys@Ca-BDC is a two-dimensional stackable sheet tens of micrometers in length and a few micrometers in thickness (Figure 2A, row 3), whereas lys@Ca-BPDC and Ca-NH_2-BPDC are also stackable sheets but smaller in size (particle diameter). Interestingly, when the enzyme is switched to lipase, the morphology became slightly different (Figure S2), where lipase@Ca-BDC composites are large cuboids but lipase@Ca-BPDC/NH_2-BPDC are smaller in size (particle diameter) with less regular shapes. This indicates that the morphology can be dependent on the enzyme (and enzyme-metal/ligand interactions) too.

An interesting finding during our X-ray diffraction (XRD) investigation is that a trace amount of protein (i.e., lysozyme) can induce the slow crystallization of Ca and BDC and generate relatively large-size single crystals (see Figure 2A). The XRD pattern of Ca-BDC (black trace in Figure 2B) is similar to that of the Ca-BDC formed in water (without protein) reported a long time ago[42] and does not match that formed under high temperature or pressure in the organic phase (without enzyme).[30] The structure of our Ca-BDC (Figure 3A; for the crystallographic information file [CIF] and details, see Tables S1 and S2 and Figure S4) indicates that each Ca^{2+} is coordinated with two oxygens from a BDC molecule in one layer and another two oxygens from two BDC

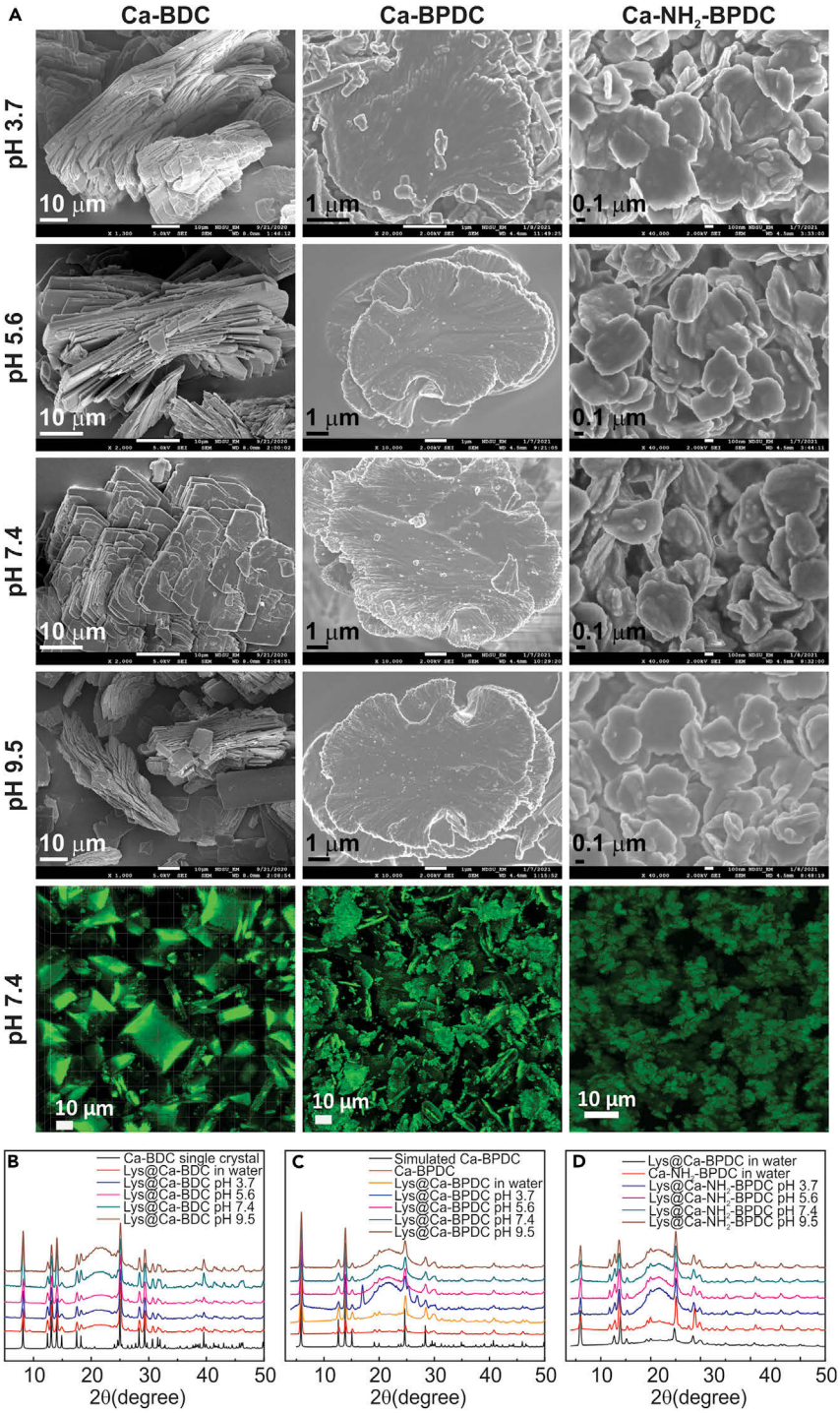

Figure 2. Acid-base stability of the enzyme@Ca-MOM composites

(A) SEM and confocal fluorescent images show stable morphologies of the enzyme@Ca-MOMs under varied pHs.

(B–D) The single-crystal XRD (B) and PXRD (C and D) patterns of the involved enzyme@Ca-MOMs confirmed the crystallinity and pH stability too. We actually obtained the Ca-BDC single crystal by scanning the single crystals of our Ca-BDC formed in the aqueous phase at room temperature. Note that this structure is different from that reported in Ca-BDC formed under higher temperature and pressure (see the main text).

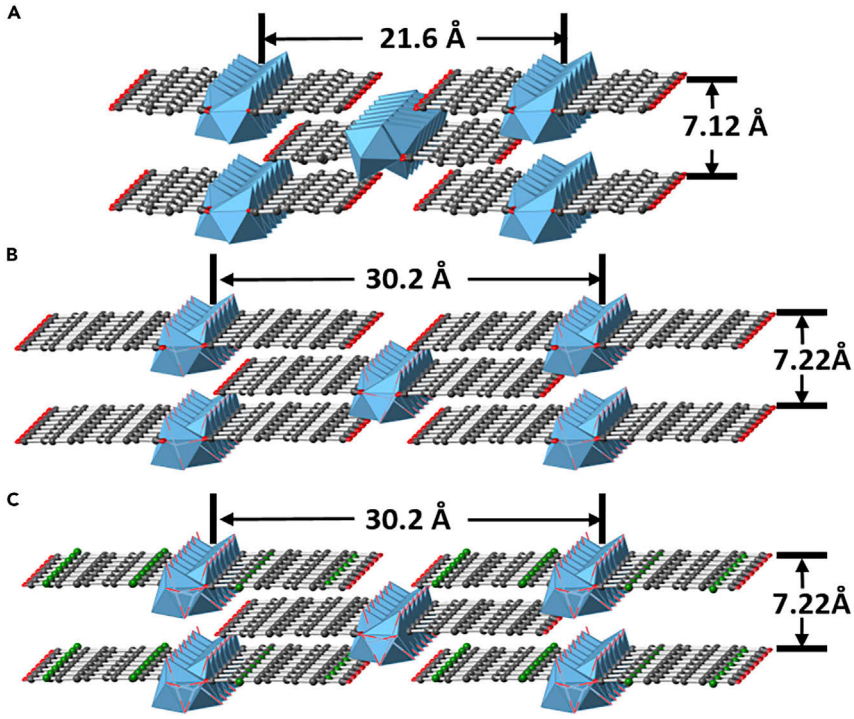

Figure 3. Crystal structures of the formed Ca-MOMs

(A) Crystal structure of Ca-BDC based on XRD data.

(B) Crystal structure of Ca-BPDC based on PXRD data.

(C) Crystal structure of Ca-NH_2-BPDC based on PXRD data.

molecules on the adjacent layer (Figure S4). In addition, four water molecules were coordinated to each Ca^{2+}. Compared with the structure acquired in the organic phase, the Ca-BDC synthesized in the aqueous phase contains two additional water molecules.[30] Loading of excess enzymes (for representative data, see lys@Ca-BDC in Figure 2B [red]) did not alter the diffraction pattern significantly. In fact, the composites were stable and capable of retaining enzyme activity (see below). However, enzyme does induce cavities and crystal defects, as indicated by the broad hump in Figure 2B. Ca-BPDC shows a powder XRD (PXRD) pattern (Figure 2C) that matches the reported structure (where Ca-MOMs were synthesized under elevated pressure and temperature in the organic phase with no enzyme). As shown in Figure 3B, Ca-BPDC scaffolds contain infinite chains of Ca^{2+} polyhedra (with 8-fold coordination: $CaO_4(H_2O)_4$ unit). The pattern of lys@Ca-NH_2-BPDC is close to that of Ca-BPDC (Figure 2D), on the basis of which the structure is derived (Figure 3C).

The co-precipitation of enzymes in Ca-MOMs was confirmed by the bicinchoninic acid (BCA) method (Figure S11). The loading capacity of lys was ~1.0%, 2.1%, and 3.3% in Ca-BDC, Ca-BPDC, and Ca-NH_2-BPDC, respectively, whereas that of lipase, GOx, and HRP in the corresponding Ca-MOMs was ~0.8%, 8.0%, and 6.4%; 6.0%, 8.2%, and 5.5%; and 4.1%, 4.6%, and 5.5%, respectively. Enzyme co-precipitation was further determined with confocal fluorescence spectroscopy. Here, the amines of each enzyme were reacted with fluorescein isothiocyanate (FITC) via the formation of a thiourea (FITC-enzyme), and then unreacted FITC was removed via filtration centrifugation. As shown by the representative data on lys@Ca-MOMs (Figure 2A, row 3 versus 5) and lipase@Ca-MOM (Figures S2 and S3), each FITC-enzyme@Ca-MOM composite displayed a shape similar to that reported by SEM, indicating

the presence of FITC-enzyme in each composite. Negative controls—enzyme@Ca-MOMs (no FITC) and Ca-MOMs (no lys)— displayed no fluorescence (data not shown), further confirming the co-precipitation of FITC-enzyme in Ca-MOMs. Thermal gravimetric analysis (TGA; for representative data on lys@Ca-MOMs, see Figure S5) also confirmed the co-precipitation of enzymes in our Ca-MOMs. The initial weight loss (100°C–170°C) was attributed to the removal of coordinated water, whereas that from 240°C to 500°C was due to the loss of entrapped lys.[14,30,43] Furthermore, Ca-MOMs with a shorter ligand (BDC) possess a higher thermal stability than those with longer ones, as indicated by the relatively higher degradation temperatures (~620°C for Ca-BDC and lys@Ca-BDC versus ~ 580°C for Ca-BPDC, Ca-NH_2-BPDC, lys@Ca-BPDC, and lys@Ca-NH_2-BPDC).

A comparison of the SEM images in the absence (Figure S18) and presence of enzyme loading suggests that enzymes can serve as the modulator of the formation of the coordination network and could thus influence the kinetics of their nucleation and crystallization. At the current moment, there is no definitive way to precisely locate enzyme positions in each composite. Because of the large size of enzymes, the enzymes can be located in the inter-particle spaces of the composite. Since these MOMs are stacked platelets, the enzymes can also be stacked and stabilized between different platelets.

Acid-base stability of enzyme@Ca-MOM composites

To evaluate the pH effects on the composites, we incubated ~2–3 μL of each stock enzyme@Ca-MOM composite (a total of 12 samples) in eight buffers (~300 μL) with a pH from 3.7 to 9.5. This pH range covers the optimal or physiological pH of most commonly encountered enzymes and was selected in our study.[25] pHs beyond this range are less biologically relevant and are beyond the scope of this study. The turbidity (optical density at 450 nm [OD450]) was monitored over time for lys@Ca-MOMs as a representative system for 3 h. As shown in Figure S6, no major drop in OD450 was observed for almost all samples, indicating that micrometer-size particles were retained under these pHs. To confirm the presence of particles, we acquired SEM images of enzyme@Ca-MOMs incubated with each buffer overnight. As shown in Figure 2A, from pH 3.7 to 9.5, the morphology of each composite upon pH change (also see Figure S1 for larger scales) after overnight incubation strongly indicates the acid-base stability of each composite. To further probe the effect of pH on the crystallinity of the enzyme@Ca-MOM composites, we acquired the XRD and PXRD data of the same samples (Figures 2B–2D), which indicated that the overall crystallinity of each composite was preserved. Other enzyme@Ca-MOMs showed similar conclusion (data not shown). Therefore, our enzyme@Ca-MOM composites are stable under a wide range of pHs (3.7–9.5).

Biocatalytic activity of the enzyme@Ca-MOM composites

Lys hydrolyzes the 1,4-glycosidic bond of bacterial cell walls, a typical large biological substrate.[44] The activity assay of lys (Sigma-Aldrich no. M3770) monitors the turbidity of bacterial cell walls upon contact with lys at OD450, a decrease in which indicates the presence of functional lys. We first demonstrated that the ligands and Ca-MOMs (without lys) did not show any cell-wall hydrolysis (Figure S7, left and middle), whereas the presence of ligands and Ca^{2+} did not affect the function of free lys (Figure S7, right). Upon quantifying the amount of lys loaded in each composite by using the BCA assay (see the supplemental information), we determined the relative activity of the free lys and lys@Ca-MOMs composites under approximately the same amount of lys in each composite. The raw data shown in Figure 4A (left) show that the free lys (black) decreased OD450 more efficiently than the three composites.

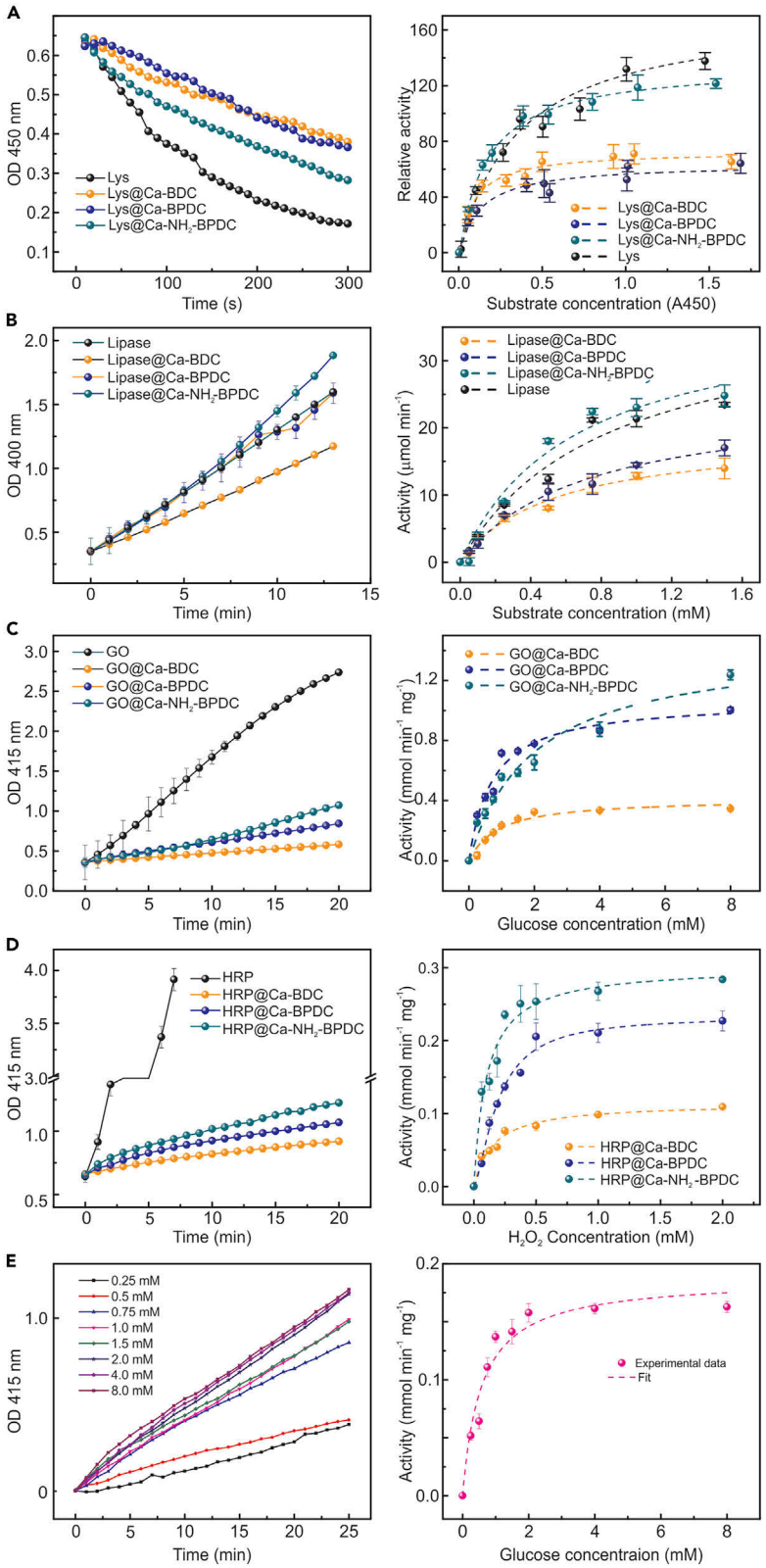
A
OD 450 nm
Time (s)
Lys
Lys@Ca-BDC
Lys@Ca-BPDC
Lys@Ca-NH2-BPDC
Relative activity
Substrate concentration (A450)
B
OD 400 nm
Time (min)
Lipase
Lipase@Ca-BDC
Lipase@Ca-BPDC
Lipase@Ca-NH2-BPDC
Activity (μmol min-1)
Substrate concentration (mM)
C
OD 415 nm
Time (min)
GO
GO@Ca-BDC
GO@Ca-BPDC
GO@Ca-NH2-BPDC
Activity (mmol min-1 mg-1)
Glucose concentration (mM)
D
OD 415 nm
Time (min)
HRP
HRP@Ca-BDC
HRP@Ca-BPDC
HRP@Ca-NH2-BPDC
Activity (mmol min-1 mg-1)
H2O2 Concentration (mM)
E
OD 415 nm
Time (min)
0.25 mM
0.5 mM
0.75 mM
1.0 mM
1.5 mM
2.0 mM
4.0 mM
8.0 mM
Activity (mmol min-1 mg-1)
Glucose concentraion (mM)
Experimental data
Fit

Figure 4. Enzyme catalytic activity upon co-precipitation in Ca-MOMs
The catalytic activity assays (left) of lys (A), lipase (B), GOx (C), HRP (D), and GOx/HRP cascade (E) and the enzymatic kinetics analysis with fitting (right) of each enzyme or enzyme cluster. The concentrations in (E) are the substrate concentrations. Error bars represent the standard deviation of three repeat measurements. For data analysis and fitting, see the main text and the supplemental information.

Furthermore, lys@Ca-NH_2-BPDC showed a higher catalytic efficiency than the other two composites. The enzymatic kinetics (Figure 4A, right; for details, see the supplemental information) also showed the same trend (V_{max} and K_m; see Table 1; through this work, error bars were the standard deviations of conducting each measurement three times under the same conditions). This result indicates that lys can be partially exposed on the surface of all three Ca-MOMs in order to contact the large substrate size, similar to our recent finding.[18] The structural basis of such activity will be analyzed later.

Another common model enzyme in biocatalysis is lipase. One of the standard lipase activity assays is to hydrolyze 4-nitrophenyl acetate and generate acetic acid and 4-nitrophenol, the latter of which has an ultraviolet-visible (UV)-vis absorption at 400 nm.[45] We first confirmed that the ligands and Ca-MOMs (without lipase) did not generate any 4-nitrophenol (Figure S8). Then, under the same enzyme amount, free lipase and three lipase@Ca-MOMs composites all showed the formation of 4-nitrophenol (Figure 4B, left). Interestingly, lipase@Ca-NH_2-BPDC showed a similar or slightly higher catalytic efficiency than free lipase in the same buffer (HEPES [pH 7.4]). The V_{max} and K_m calculations (Figure 4B, right, and Table 2) also indicated the same trend. The high lipase activity in Ca-NH_2-BPDC was most likely caused by the enhanced backbone dynamics of the protein in this MOM (see structural analysis below); further investigation on lipase dynamics is needed to clarify this point, which is one of our ongoing research directions.

GOx and HRP are frequently used for testing cascade biocatalysis and were therefore studied here. GOx activity was determined together with HRP.[46,47] In brief, GOx degrades glucose into glucono-lactone and H_2O_2; the generated H_2O_2 and HRP then convert the 2,2′-azino-bis(3-ethylbenzothiazoline-6-sulfonic acid) diammonium salt (ABTS) to $ABTS^{+\bullet}$, which has a UV-vis absorption at 415 nm.[48,49] After we confirmed that the ligands and Ca-MOMs (without GOx) did not generate any $ABTS^{+\bullet}$ (in the presence of free HRP Figure S10), under the same GOx amount, free GOx and three GOx@Ca-MOMs composites showed the formation of $ABTS^{+\bullet}$ (Figure 4C, left), although the efficiency was much lower in the composites than in free GOx, most likely because of the reduced enzyme mobility and substrate diffusivity. Interestingly, the same trend of relative activity among the composites was found: GOx@Ca-BDC < GOx@Ca-BPDC < GOx@Ca-NH_2-BPDC (also see Figure 4C, right, and Table 3).

HRP activity was studied similarly except that H_2O_2 was provided to free HRP and HRP@Ca-MOM composites. Similarly, a trend of relative activity among the three

Table 1. The kinetic parameters of the hydrolysis of *Micrococcus lysodeikticus* cell walls catalyzed by the lys@Ca-MOM composites obtained via the Michaelis-Menten method

Parameters	V_{max} (μmol/min)	K_m (μM)	R^2
Lys	173.7 ± 16.8	0.36 ± 0.10	0.964
lys@Ca-BDC	72.8 ± 2.68	0.087 ± 0.016	0.974
lys@Ca-BPDC	63.8 ± 3.8	0.130 ± 0.036	0.947
lys@Ca-NH_2-BPDC	135.2 ± 2.8	0.171 ± 0.013	0.959

Table 2. The kinetic parameters of free lipase and the synthesized lipase@Ca-MOM composites

Parameters	V_{max} (μmol/min)	K_m (μM)	R^2
Lipase	38.21 ± 5.92	0.83 ± 0.26	0.987
lipase@Ca-BDC	19.10 ± 1.47	0.53 ± 0.10	0.984
lipase@Ca-BPDC	24.63 ± 1.70	0.71 ± 0.00	0.979
lipase@Ca-NH_2-BPDC	37.86 ± 5.27	0.65 ± 0.20	0.988

composites was observed (Figure 4D, right, and Table 3). Lastly, GOx and HRP were encapsulated together in Ca-BPDC. As shown in Figure 4E, cascade biocatalysis reactions occurred in the composites, demonstrating the feasibility of using our composites for multiple enzyme co-precipitation and cascade biocatalysis.

All catalytic assays discussed above were carried out under the suggested buffer condition in the assay. To confirm that our Ca-MOMs can conduct catalysis under different pHs for the same enzyme, we selected lipase@Ca-MOMs as a representative under pH 6.8–8.2 in HEPES buffer. This pH range can be tolerated by the HEPES buffer (for activity comparison); representative data in other buffers that can offer different pHs are shown in Figure S9. Note that we did not compare the relative activity in different buffers because buffer composition can also affect the catalytic efficiency of enzymes.[50,51] As shown in Figures S12A–S12C, all three composites showed a higher activity at pH 7.4 and 8.2 than at pH 6.8. Note that catalytic activity was observed under even lower or higher pHs (data not shown); however, because of the general buffer dependence of enzymes, we did not compare the catalytic efficiency of lipase@Ca-MOMs among buffers with different composition. To confirm the stability of the composites after biocatalysis, we repeated the catalytic cycle for each lipase@Ca-MOMs six times (under HEPES buffer at pH 7.4). As shown in Figure S12D, >90% relative activity was reserved after six repeated cycles, indicating the stability of our composites after multiple catalytic cycles.

DISCUSSION

The structural basis of biocatalysis

Two interesting observations require some in-depth thinking: the origin of the lys activity against a large substrate and why most enzymes show the best activity in Ca-NH_2-BPDC. Because of the close structure-function relationship of enzymes, we decided to probe the structural basis of our enzyme@Ca-MOM composites. We chose lys as our pilot system because of its extensively studied structure-function relationship. Because of the complexities caused by the Ca-MOM backgrounds, which complicate the data analysis of most enzyme structure probing techniques, we selected SDSL-EPR. As a technique based on magnetic resonance, the "penetrating" power of EPR probes only the paramagnetic species (unpaired electrons) to reveal the relevant structural information regardless of the background

Table 3. The kinetic parameters of the GOx@Ca-MOM, HRP@Ca-MOM, and GOx/HRP@Ca-BPDC composites

Parameters	V_{max} (mmol min^{-1} mg^{-1})	K_m (mM)	R^2
GOx@Ca-BDC	0.41 ± 0.03	0.88 ± 0.21	0.949
GOx@Ca-BPDC	1.07 ± 0.05	0.72 ± 0.12	0.972
GOx@Ca-NH_2-BPDC	1.45 ± 0.12	2.00 ± 0.40	0.962
HRP@Ca-BDC	0.57 ± 0.03	0.62 ± 0.11	0.972
HRP@Ca-BPDC	1.33 ± 0.08	1.00 ± 0.18	0.969
HRP@Ca-NH_2-BPDC	1.51 ± 0.07	0.41 ± 0.08	0.967
GOx/HRP@Ca-BPDC	0.91 ± 0.01	0.57 ± 0.13	0.948

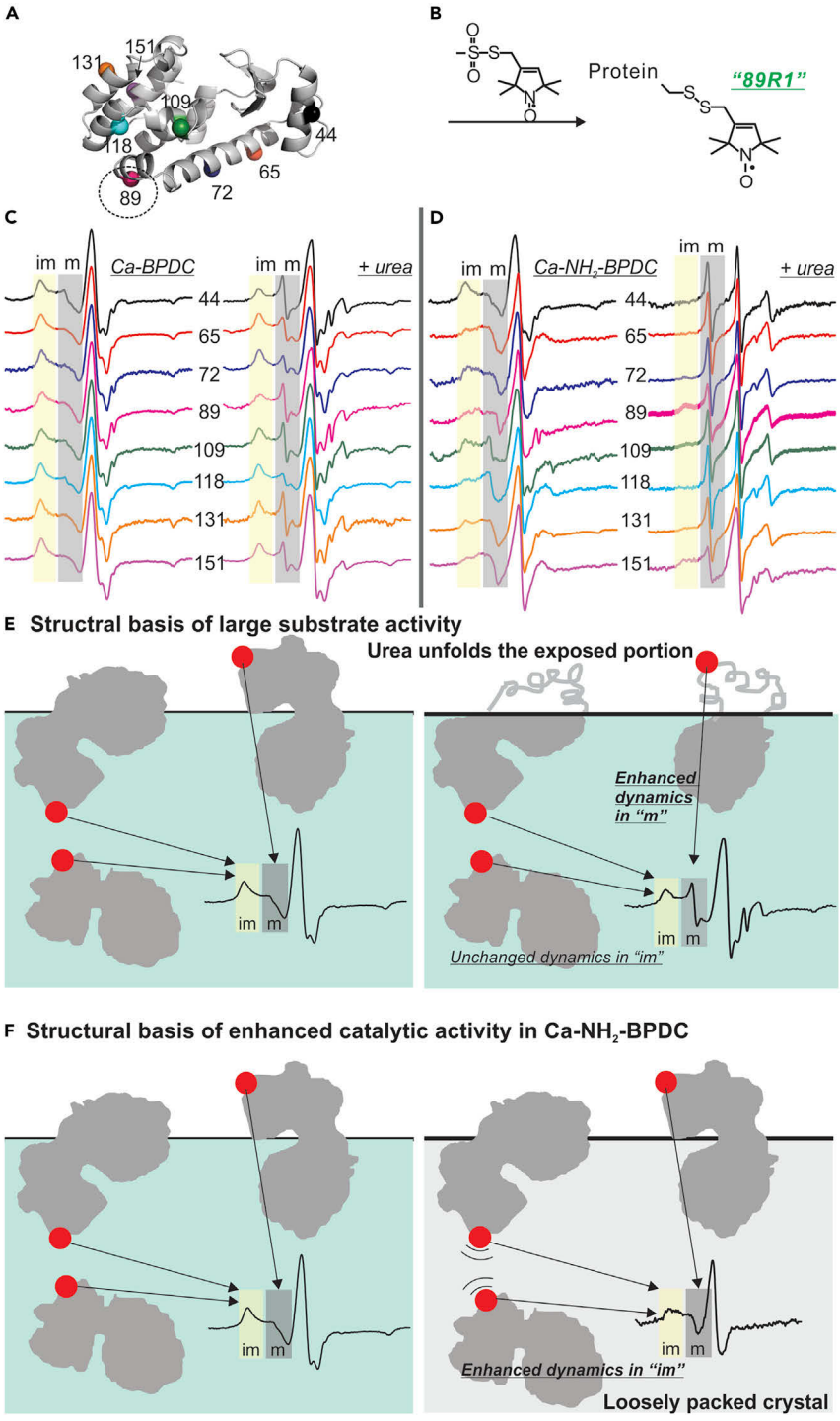

Figure 5. Probing the structural basis of the catalytic performance of enzyme@Ca-MOM composites

(A) Eight surface sites of T4L studied in this work.

(B) SDSL of a representative site (89C) of T4L with R1.

(C and D) EPR spectra of all labeled sites in the absence (left) and presence (right) of urea for lys@Ca-BPDC and lys@Ca-NH_2-BPDC. Shades indicate the two spectral components discussed in the text. Spectral range: 3,300–3,400 G.

Figure 5. *Continued*
(E) Illustration of EPR detection of the exposed (m spectral component) and buried (im spectral component) enzyme upon co-precipitation on MOM surfaces (left) and upon treatment of urea, which only unfolds the exposed portion of the enzyme (right). (F) Illustration of EPR detection of the backbone dynamics of the buried (im spectral component) enzyme.

complexities or structural heterogeneities of the target system. Because most proteins are diamagnetic, spin labeling is needed. SDSL of protein allows a spin label to be attached at a specific residue of the target enzyme. Thus, combining SDSL and EPR can, in principle, reveal enzyme structural information at residue-level resolution.

A key structural information related to enzyme activity is the backbone dynamics of the labeled site, which is typically ~nanosecond order and can be revealed by continuous wave (CW) EPR, whose typical resonance frequency is ~gigahertz. Within such a time window, the CW EPR line shape is sensitive to the rate and order of the motion of the spin label so that a label in fast motion often results in a sharp spectrum (usually three sharp first-derivative peaks due to the hyperfine splitting of the N nucleus in the spin label; see supplemental experimental procedures and Figures S16A1 and A2), as in the case of a small globular enzyme in solution. As the motion of the protein is slowed down, such as upon immobilization in MOMs, the spectrum becomes broader (Figure S16A3; often defined as the mobile [m] component). Furthermore, when the labeled site is in contact with some species (e.g., the MOM scaffolds), the space allowed for the label to move is restricted (high order), leading to an even broader overall spectrum (see Figure S16A4; often defined as the immobile [im] component). The higher the degree of restriction, the narrower the low-field peak (see Figure S16A5 versus Figure S16A4). Therefore, by probing the EPR spectrum of a labeled enzyme site, it is possible to determine whether the enzyme is immobilized on MOMs and whether the labeled site is buried under the MOM surface or exposed above. When two cases simultaneously occur in an ensemble, a complex EPR spectrum (usually with two spectral components) can be resolved; the contribution from each component can be deconvoluted via spectral simulation (Figure S17).[50] Lastly, by scanning the labeled site through the target enzyme, it is possible to determine the regions of the enzyme being buried or exposed, whereas by comparing the im component, it is possible to compare the relative degree of spatial restriction for a labeled site contacting different species (Figure S16A5 versus Figure S16A4).

To understand our data, we applied a principle similar to that reported in our recent work.[19] In brief, upon SDSL, an enzyme, e.g., lys (Figure 5A and 5B), can be buried in the MOM scaffolds as well as partially exposed to the reaction medium. The exposed residues display enhanced dynamics compared with those buried under the composite surface. When the same residue is exposed in some enzyme molecules but buried in others, a heterogeneous spectrum will be resolved with a more dynamic m component and a more restricted im component, respectively (Figures 5C and 5D, left). The contribution of each component can be quantified via spectral simulation.[33,52] Furthermore, an urea-unfolding test can be applied to confirm the presence of exposed enzyme regions and their relative contribution because urea only unfolds the exposed areas of an enzyme (Figures 5C and 5D, right, and Figure 5E).[19,53,54] A labeled residue showing an enhanced m component upon urea treatment has a higher chance of being exposed.

On the basis of these principles, we carried out SDSL-EPR study on eight residues of the lys covering most lys surfaces (Figure 5A). Upon confirming that the mutation and

spin label did not alter protein secondary structure and function (Figures S13–S15), we found that for all spectra, both im and m components were observed (Figures 5C and 5D, left, yellow and gray shades, respectively), indicating that in the whole composite, most enzyme regions can be both exposed and buried in others. The spectra of lys@Ca-BDC (Figure S16, left) and lys@Ca-BPDC (Figure 5C, left) are similar to each other but have subtle differences in the intensity of the im component. The spectra of lys@Ca-NH_2-BPDC are greatly different from those of the other two Ca-MOMs by the enhanced intensity of the m and broadened im peaks (Figure 5D, left). Upon treatment of urea, all lys@Ca-MOMs show m components with sharpened derivative peaks (Figures 5C and 5D, right), confirming that almost all sites can be partially exposed to the reaction medium. Thus, the active site of lys can also be exposed (at least partially), which allows for contacting with the large-size substrate, bacterial cell walls. The smaller size (particle diameter) of lys@Ca-NH_2-BPDC (Figure 2), together with the enhanced mobility (the enhanced m component), is the likely cause of the higher catalytic efficiency against the cell walls (due to enhanced contact probability with the cell walls) than of the other lys@Ca-MOM composites.

Possible rationalization of the high enzyme activity in Ca-NH_2-BPDC

Because the substrates of lipase, GOx, and HRP are small molecules, composite size differences cannot explain the activity differences upon ligand change. However, such activity differences might still originate from the structure-function relationship of enzymes. We thus probed the backbone dynamics of the enzymes buried under the surface of the Ca-MOMs since the buried portion is the major contribution to the catalysis of small substrates. As explained above, the im component of an EPR spectrum is caused by a labeled enzyme site buried under MOM surfaces. Thus, we carefully analyzed this component by varying the rate and order parameter of each component as well as their relative fractions to reach a best fit to each spectrum (see details in the supplemental information). The best rate and order parameters reflect the frequency and spatial confinement of a spectral component (either m or im), respectively, which, as shown in Tables S3–S5, indicate higher enzyme backbone dynamics at each labeled site in lys@Ca-NH_2-BPDC (faster rate [larger R values] and lower order [lower C values] or higher spatial freedom) than in lys@Ca-BDC and lys@Ca-BPDC. Thus, as illustrated in Figure 5F, lys buried under the surface of the Ca-NH_2-BPDC has higher backbone dynamics than that under the surface of Ca-BPDC or Ca-BDC. As shown in our recent work, enhanced backbone dynamics or conformational degree of freedom favors enzymes to carry out their catalytic functions.[55] Compared with Ca-BDC and Ca-BPDC, the additional NH_2 groups in the ligand (and thus among the gaps between the layers) may offer a protein/enzyme-friendly environment that helps retain protein intrinsic dynamics and/or conformational freedom. These enhanced dynamics, as suggested by our EPR data on lys@Ca-MOMs, are most likely responsible for the enhanced catalytic efficiency. Therefore, we speculate that this is the same cause of the higher catalytic efficiency of the other two enzymes in Ca-NH_2-BPDC than of the other two Ca-MOMs. SDSL-EPR studies of these three enzymes are our ongoing work. Note that one out of the four studied enzymes did not show the trend of the relative catalytic efficiency among the three Ca-MOMs. This also indicates that the catalytic efficiency or functionality of enzymes trapped in MOMs is likely to be complex and dependent on a number of factors. For example, the enzyme content in Ca-NH_2-BPDC is about three times higher than in the other composites, whereas the particle size of Ca-NH_2-BPDC is significantly smaller. This means that the confinement (density) of enzyme is presumably higher in Ca-NH_2-BPDC than in the other composites, which could lead to the enhanced catalytic efficiency. Moreover, because of the smaller diameter of Ca-NH_2-BPDC particles than of the other composites and the possible presence

of NH_2 groups at the surface of specific facets of the Ca-NH_2-BPDC particles, the interactions between enzymes and Ca-NH_2-BPDC particles can be different from those in the other composites as a result of a difference in surface chemistry of the coordination networks. Such interactions could result in different conformation, tertiary structure, and activity of proteins, as shown in the immobilization of laccase in carbon-based materials.[56,57] Thus, predicting the catalytic performance of the trapped enzymes solely on the basis of ligands, metal ions, crystal structures and cavities, and/or composite morphology is difficult. A thorough characterization of enzyme dynamics is needed, which is our on-going work.

Altogether, we came up with a schematic model that explains the catalytic performance of the involved enzymes in each Ca-MOM. For small substrates, the enzyme encapsulated inside of the Ca-NH_2-BPDC possesses enhanced dynamics and therefore enhanced relative catalytic efficiency compared with that of the same enzyme in the other two Ca-MOMs. For larger substrates, the partial exposure of the enzyme (lys) allows their contact with the substrates and thus leads to hydrolysis (breakage) of the cell walls.

In this work, we named the obtained composites as MOMs according to the definition,[58] although MOF has been used as well.[30] This one-dimensional coordination platform is most likely applicable to other large-substrate enzymes, such as α-amylase, as indicated by one of our recent works.[59]

In conclusion, we report the co-precipitation of three carboxylate ligands—BDC, BPDC, and NH_2-BPDC—with enzymes and Ca^{2+} in water via one-pot synthesis. The aqueous reaction medium minimized enzyme damage during co-precipitation while allowing for the entrapment of enzymes with varied isoelectric points (surface charges), molecular weights, and substrate sizes. Remarkably, the resultant enzyme@Ca-MOM composites are stable over a wide range of pHs (3.7–9.5), which opens an avenue of conducing biocatalysis under the optimal pHs of different enzymes. We tested the generality of our platform on four commonly used enzymes in biocatalysis and found that all enzymes displayed expected activities. Interestingly, for three of the four enzymes, we found that the catalytic efficiency is highest in Ca-NH_2-BPDC regardless of the substrate size, the structural basis of which was probed by SDSL-EPR. Our data suggest that in Ca-NH_2-BPDC, the enzymes displayed enhanced backbone dynamics, which was suggested to be the cause of the high activity for enzymes trapped therein. Our approach can be generalized to other enzymes with arbitrary protein and substrate sizes for carrying out biocatalysis under various pHs. The ease of operation and the ambient reaction conditions are also advantageous for industrial biocatalyst preparation.

EXPERIMENTAL PROCEDURES

Resource availability

Lead contact

Further information and requests for resources and reagents should be directed to and will be fulfilled by the lead contact, Zhongyu Yang (zhongyu.yang@ndsu.edu).

Materials availability

All unique and stable reagents generated in this study are available from the lead contact without restriction.

Data and code availability

The CIF of the crystal structure of Ca-BDC has been deposited to the Cambridge Crystallographic Data Centre (CCDC) (Datablock: p21c; CCDC: 1987259). The EPR

data supporting the current study have not been deposited in a public repository because of the lack of a proper data resource but are available from the lead contact on request.

Materials and measurements

All chemicals and biochemical supplies were purchased from commercial sources in high purity; the involved experiments were carried out without purification. All characterization, including PXRD, single-crystal XRD, SEM, TGA, and ^{1}H-NMR spectroscopy, of the involved materials followed the published procedures using equipment described in our recent work.[53] The expression, purification, and spin labeling of involved lysozyme mutants followed the procedures described in our recent work.[19] For EPR measurements, each protein mutant was transferred into a borosilicate capillary tube (0.70 mm inside diameter, 1.00 mm outside diameter; Wilmad Labglass) immediately after the channel materials were mixed. Data were acquired with a Varian E-109 spectrometer equipped with a cavity resonator. All CW EPR spectra were obtained with an observe power of 200 mW, a modulation frequency of 100 kHz, and a modulation amplitude of 1.0 G.

SUPPLEMENTAL INFORMATION

Supplemental information can be found online at https://doi.org/10.1016/j.checat.2021.03.001.

ACKNOWLEDGMENTS

This work was supported by the National Science Foundation (grant MCB 1942596 to Z.Y.), North Dakota State University New Faculty Startup Funds, and USDA-NIFA grant 2021-67021-34002 (to B.C.). We appreciate Prof. Hubbell for generously providing the EPR spectral simulation package.

AUTHOR CONTRIBUTIONS

Z.L, B.C., and Z.Y. conceived and designed the research. Y.P. and Q.L. performed the synthesis and catalytic assays. Y.P., H.L., and J.F. acquired the EPR data and carried out the data analysis. A.U. and X.Z. assisted in all data analysis and interpretation. All authors participated in drafting the manuscript and gave approval to the final version.

DECLARATION OF INTERESTS

The authors declare no competing interests.

Received: November 11, 2020
Revised: January 13, 2021
Accepted: March 2, 2021
Published: April 23, 2021

REFERENCES

1. Nel, A.E., Mädler, L., Velegol, D., Xia, T., Hoek, E.M.V., Somasundaran, P., Klaessig, F., Castranova, V., and Thompson, M. (2009). Understanding biophysicochemical interactions at the nano-bio interface. Nat. Mater. *8*, 543–557.

2. Küchler, A., Yoshimoto, M., Luginbühl, S., Mavelli, F., and Walde, P. (2016). Enzymatic reactions in confined environments. Nat. Nanotechnol. *11*, 409–420.

3. Sheldon, R.A., and Woodley, J.M. (2018). Role of biocatalysis in sustainable chemistry. Chem. Rev. *118*, 801–838.

4. Chapman, R., and Stenzel, M.H. (2019). All wrapped up: stabilization of enzymes within single enzyme nanoparticles. J. Am. Chem. Soc. *141*, 2754–2769.

5. Shemetov, A.A., Nabiev, I., and Sukhanova, A. (2012). Molecular interaction of proteins and peptides with nanoparticles. ACS Nano *6*, 4585–4602.

6. Wang, X., Lan, P.C., and Ma, S. (2020). Metal-organic frameworks for enzyme immobilization: beyond host matrix materials. ACS Cent. Sci. *6*, 1497–1506.

7. Lian, X., Fang, Y., Joseph, E., Wang, Q., Li, J., Banerjee, S., Lollar, C., Wang, X., and Zhou, H.-C. (2017). Enzyme-MOF (metal-organic

framework) composites. Chem. Soc. Rev. *46*, 3386–3401.

8. Drout, R.J., Robison, L., and Farha, O.K. (2019). Catalytic applications of enzymes encapsulated in metal-organic frameworks. Coord. Chem. Rev. *381*, 151–160.

9. Majewski, M.B., Howarth, A.J., Li, P., Wasielewski, M.R., Hupp, J.T., and Farha, O.K. (2017). Enzyme encapsulation in metal-organic frameworks for applications in catalysis. CrystEngComm *19*, 4082–4091.

10. Howarth, A.J., Liu, Y., Li, P., Li, Z., Wang, T.C., Hupp, J.T., and Farha, O.K. (2016). Chemical, thermal and mechanical stabilities of metal-organic frameworks. Nat. Rev. Mater. *1*, 15018.

11. Gkaniatsou, E., Sicard, C.m., Ricoux, R.m., Mahy, J.-P., Steunou, N., and Serre, C. (2017). Metal-organic frameworks: a novel host platform for enzymatic catalysis and detection. Mater. Horiz. *4*, 55–63.

12. Fang, Y., Powell, J.A., Li, E., Wang, Q., Perry, Z., Kirchon, A., Yang, X., Xiao, Z., Zhu, C., Zhang, et al.. (2019). Catalytic reactions within the cavity of coordination cages. Chem. Soc. Rev. *48*, 4707–4730.

13. Mehta, J., Bhardwaj, N., Bhardwaj, S.K., Kim, K.H., and Deep, A. (2016). Recent advances in enzyme immobilization techniques: metal-organic frameworks as novel substrates. Coord. Chem. Rev. *322*, 30–40.

14. Lyu, F., Zhang, Y., Zare, R.N., Ge, J., and Liu, Z. (2014). One-pot synthesis of protein-embedded-supporting information. Nano Lett. *14*, 5761–5765.

15. Liang, W., Xu, H., Carraro, F., Maddigan, N.K., Li, Q., Bell, S.G., Huang, D.M., Tarzia, A., Solomon, M.B., Amenitsch, H., et al. (2019). Enhanced activity of enzymes encapsulated in hydrophilic metal-organic frameworks. J. Am. Chem. Soc. *141*, 2348–2355.

16. An, H., Song, J., Wang, T., Xiao, N., Zhang, Z., Cheng, P., Huang, H., Ma, S., and Chen, Y. (2020). Metal-organic framework disintegrants: a new generation of enzyme preparation platforms with boosted activity. Angew. Chem. Int. Ed. https://doi.org/10.1002/anie.202007827.

17. Saliba, D., Ammar, M., Rammal, M., Al-Ghoul, M., and Hmadeh, M. (2018). Crystal growth of ZIF-8, ZIF-67, and their mixed-metal derivatives. J. Am. Chem. Soc. *140*, 1812–1823.

18. Cravillon, J., Schröder, C.A., Nayuk, R., Gummel, J., Huber, K., and Wiebcke, M. (2011). Fast nucleation and growth of ZIF-8 nanocrystals monitored by time-resolved in situ small-angle and wide-angle X-ray scattering. Angew. Chem. Inter. Ed. *50*, 8067–8071.

19. Pan, Y., Li, H., Farmakes, J., Xiao, F., Chen, B., Ma, S., and Yang, Z. (2018). How do enzymes orient on metal-organic framework (MOF) surfaces? J. Am. Chem. Soc. *140*, 16032–16036.

20. Neupane, S., Patnode, K., Li, H., Baryeh, K., Liu, G., Hu, J., Chen, B., Pan, Y., and Yang, Z. (2019). Enhancing enzyme immobilization on carbon nanotubes via metal-organic frameworks for large-substrate biocatalysis. ACS Appl. Mater. Inter. *11*, 12133–12141.

21. Farmakes, J., Schuster, I., Overby, A., Alhalhooly, L., Lenertz, M., Li, Q., Ugrinov, A., Choi, Y., Pan, Y., and Yang, Z. (2020). Enzyme immobilization on graphene oxide (GO) surface via one-pot synthesis of GO/metal-organic framework composites for large-substrate biocatalysis. ACS Appl. Mater. Inter. *12*, 23119–23126.

22. Gao, S., Hou, J., Deng, Z., Wang, T., Beyer, S., Buzanich, A., Richardson, J.J., Rawal, A., Seidel, R., Zulkifli, M., et al. (2019). Improving the acidic stability of zeolitic imidazolate frameworks by biofunctional molecules. Chem *5*, 1597–1608.

23. Wei, T.-H., Wu, S.-H., Huang, Y.-D., Lo, W.-S., Williams, B.P., Chen, S.-Y., Yang, H.-C., Hsu, Y.-S., Lin, Z.-Y., Chen, X.-H., et al. (2019). Rapid mechanochemical encapsulation of biocatalysts into robust metal-organic frameworks. Nat. Commun. *10*, 5002.

24. Bai, Y., Dou, Y., Xie, L.-H., Rutledge, W., Li, J.-R., and Zhou, H.-C. (2016). Zr-based metal-organic frameworks: design, synthesis, structure, and applications. Chem. Soc. Rev. *45*, 2327–2367.

25. Talley, K., and Alexov, E. (2010). On the pH-optimum of activity and stability of proteins. Proteins: Struct. Funct. Bioinf. *78*, 2699–2706.

26. Lin, R.-B., Li, L., Zhou, H.-L., Wu, H., He, C., Li, S., Krishna, R., Li, J., Zhou, W., and Chen, B. (2018). Molecular sieving of ethylene from ethane using a rigid metal-organic framework. Nat. Mater. *17*, 1128–1133.

27. Chen, X., Plonka, A.M., Banerjee, D., Krishna, R., Schaef, H.T., Ghose, S., Thallapally, P.K., and Parise, J.B. (2015). Direct observation of Xe and Kr adsorption in a Xe-selective microporous metal-organic framework. J. Am. Chem. Soc. *137*, 7007–7010.

28. Yang, J., Trickett, C.A., Alahmadi, S.B., Alshammari, A.S., and Yaghi, O.M. (2017). Calcium l-lactate frameworks as naturally degradable carriers for pesticides. J. Am. Chem. Soc. *139*, 8118–8121.

29. Banerjee, D., Simon, C.M., Plonka, A.M., Motkuri, R.K., Liu, J., Chen, X., Smit, B., Parise, J.B., Haranczyk, M., and Thallapally, P.K. (2016). Metal-organic framework with optimally selective xenon adsorption and separation. Nat. Commun. *7*, 11831.

30. Sumida, K., Hu, M., Furukawa, S., and Kitagawa, S. (2016). Structuralization of Ca2+-based metal-organic frameworks prepared via coordination replication of calcium carbonate. Inorg. Chem. *55*, 3700–3705.

31. Mazaj, M., Mali, G., Rangus, M., Žunkovič, E., Kaučič, V.e., and Zabukovec Logar, N.a. (2013). Spectroscopic studies of structural dynamics induced by heating and hydration: a case of calcium-terephthalate metal-organic framework. J. Phys. Chem. C *117*, 7552–7564.

32. Miller, S.R., Alvarez, E., Fradcourt, L., Devic, T., Wuttke, S., Wheatley, P.S., Steunou, N., Bonhomme, C., Gervais, C., Laurencin, D., et al. (2013). A rare example of a porous Ca-MOF for the controlled release of biologically active NO. Chem. Commun. *49*, 7773–7775.

33. Hubbell, W.L., López, C.J., Altenbach, C., and Yang, Z. (2013). Technological advances in site-directed spin labeling of proteins. Curr. Opin. Struct. Biol. *23*, 725–733.

34. Cafiso, D.S. (2014). Identifying and quantitating conformational exchange in membrane proteins using site-directed spin labeling. Acc. Chem. Res. *47*, 3102–3109.

35. Fanucci, G.E., and Cafiso, D.S. (2006). Recent advances and applications of site-directed spin labeling. Curr. Opin. Struct. Biol. *16*, 644–653.

36. Qin, P.Z., Haworth, I.S., Cai, Q., Kusnetzow, A.K., Grant, G.P.G., Price, E.A., Sowa, G.Z., Popova, A., Herreros, B., and He, H. (2007). Measuring nanometer distances in nucleic acids using a sequence-independent nitroxide probe. Nat. Protoc. *2*, 2354–2365.

37. McHaourab, H.S., Steed, P.R., and Kazmier, K. (2011). Toward the fourth dimension of membrane protein structure: insight into dynamics from spin-labeling EPR spectroscopy. Structure *19*, 1549–1561.

38. DeBerg, H.A., Brzovic, P.S., Flynn, G.E., Zagotta, W.N., and Stoll, S. (2016). Structure and energetics of allosteric regulation of HCN2 ion channels by cyclic nucleotides. J. Biol. Chem. *291*, 371–381.

39. Neupane, S., Pan, Y., Li, H., Patnode, K., Farmakes, J., Liu, G., and Yang, Z. (2018). Engineering protein-gold nanoparticle/nanorod complexation via surface modification for protein immobilization and potential therapeutic applications. ACS Appl. Nano Mater. *1*, 4053–4063.

40. Altenbach, C., López, C.J., Hideg, K., Hubbell, W.L., Peter, Z.Q., and Kurt, W. (2015). Chapter three - exploring structure, dynamics, and topology of nitroxide spin-labeled proteins using continuous-wave electron paramagnetic resonance spectroscopy. Methods Enzymol. *564*, 59–100.

41. Chen, Y., Li, P., Zhou, J., Buru, C.T., Đorđevi, L., Li, P., Zhang, X., Cetin, M.M., Stoddart, J.F., Stupp, S.I., et al. (2020). Integration of enzymes and photosensitizers in a hierarchical mesoporous metal-organic framework for light-driven CO_2 reduction. J. Am. Chem. Soc. *142*, 1768–1773.

42. Matsuzaki, T., and Iitaka, Y. (1972). The crystal structure of calcium terephthalate trihydrate. Acta Crystallogr. Section B *28*, 1977–1981.

43. Li, P., Chen, Q., Wang, T.C., Vermeulen, N.A., Mehdi, B.L., Dohnalkova, A., Browning, N.D., Shen, D., Anderson, R., Gómez-Gualdrón, D.A., et al. (2018). Hierarchically engineered mesoporous metal-organic frameworks toward cell-free immobilized enzyme systems. Chem *4*, 1022–1034.

44. Vocadlo, D.J., Davies, G.J., Laine, R., and Withers, S.G. (2001). Catalysis by hen egg-white lysozyme proceeds via a covalent intermediate. Nature *412*, 835–838.

45. Nie, K., An, Q., and Zhang, Y. (2016). A functional protein retention and release multilayer with high stability. Nanoscale *8*, 8791–8797.

46. Chen, W.-H., Vázquez-González, M., Zoabi, A., Abu-Reziq, R., and Willner, I. (2018). Biocatalytic cascades driven by enzymes encapsulated in metal-organic framework nanoparticles. Nat. Catal. *1*, 689–695.

47. Zhang, Y., Tsitkov, S., and Hess, H. (2016). Proximity does not contribute to activity

enhancement in the glucose oxidase-horseradish peroxidase cascade. Nat. Commun. *7*, 13982.

48. Zhang, Y., and Hess, H. (2020). Inhibitors in commercially available 2,2′-azino-bis(3-ethylbenzothiazoline-6-sulfonate) affect enzymatic assays. Anal. Chem. *92*, 1502–1510.

49. Xiong, Y., Huang, J., Wang, S.-T., Zafar, S., and Gang, O. (2020). Local environment affects the activity of enzymes on a 3D molecular scaffold. ACS Nano *14*, 14646–14654.

50. Kuo, C.-H., Liu, Y.-C., Chang, C.J., Chen, J.-H., Chang, C., and Shieh, C.-J. (2012). Optimum conditions for lipase immobilization on chitosan-coated Fe_3O_4 nanoparticles. Carbohydr. Polym. *87*, 2538–2545.

51. Park, C., and Raines, R. (2001). Quantitative analysis of the effect of salt concentration on enzymatic catalysis *123*, 11472–11479.

52. Budil, D.E., Lee, S., Saxena, S., and Freed, J.H. (1996). Nonlinear-least-squares analysis of slow-motion EPR spectra in one and two dimensions using a modified Levenberg-Marquardt algorithm. J. Magn. Reson. A. *120*, 155–189.

53. Bennion, B.J., and Daggett, V. (2003). The molecular basis for the chemical denaturation of proteins by urea. Proc. Natl. Acad. Sci. *100*, 5142.

54. Liao, F.S., Lo, W.S., Hsu, Y.S., Wu, C.C., Wang, S.C., Shieh, F.K., Morabito, J.V., Chou, L.Y., Wu, K.C.W., and Tsung, C.K. (2017). Shielding against unfolding by embedding enzymes in metal-organic frameworks via a de novo approach. J. Am. Chem. Soc. *139*, 6530–6533.

55. Sun, Q., Pan, Y., Wang, X., Li, H., Farmakes, J., Aguila, B., Yang, Z., and Ma, S. (2019). Mapping out the degree of freedom of hosted enzymes in confined spatial environments. Chem *5*, 3184–3195.

56. Benzaqui, M., Semino, R., Carn, F., Tavares, S.R., Menguy, N., Giménez-Marqués, M., Bellido, E., Horcajada, P., Berthelot, T., Kuzminova, A.I., et al. (2019). Covalent and selective grafting of polyethylene glycol brushes at the surface of ZIF-8 for the processing of membranes for pervaporation. ACS Sustain. Chem. Engineer. *7*, 6629–6639.

57. Gkaniatsou, E., Ricoux, R., Kariyawasam, K., Stenger, I., Fan, B., Ayoub, N., Salas, S., Patriarche, G., Serre, C., Mahy, J.-P., et al. (2020). Encapsulation of microperoxidase-8 in MIL-101(Cr)-X nanoparticles: influence of metal–organic framework functionalization on enzymatic immobilization and catalytic activity. ACS Appl. Nano Mater. *3*, 3233–3243.

58. Seth, S., and Matzger, A.J. (2017). Metal-organic frameworks: examples, counterexamples, and an actionable definition. Cryst. Growth Des. *17*, 4043–4048.

59. Li, Q., Pan, Y., Li, H., Alhalhooly, L., Li, Y., Chen, B., Choi, Y., and Yang, Z. (2020). Size-tunable metal–organic framework-coated magnetic nanoparticles for enzyme encapsulation and large-substrate biocatalysis. ACS Appl. Mater. Inter. *12*, 41794–41801.